

Copyright © 2006, Paper 10-017; 10,297 words, 7 Figures, 0 Animations, 4 Tables.
<http://EarthInteractions.org>

Feedbacks of Vegetation on Summertime Climate Variability over the North American Grasslands. Part I: Statistical Analysis

**Weile Wang,* Bruce T. Anderson, Nathan Phillips, and
Robert K. Kaufmann**

Department of Geography and Environment, Boston University, Boston, Massachusetts

Christopher Potter

Ecosystem Science and Technology Branch, NASA Ames Research Center,
Moffett Field, California

Ranga B. Myneni

Department of Geography and Environment, Boston University, Boston, Massachusetts

Received 27 January 2006; accepted 28 June 2006

ABSTRACT: Feedbacks of vegetation on summertime climate variability over the North American Grasslands are analyzed using the statistical technique of Granger causality. Results indicate that normalized difference vegetation index (NDVI) anomalies early in the growing season have a statistically measurable effect on precipitation and surface temperature later in summer. In particular, higher means and/or decreasing trends of NDVI anomalies tend to

* Corresponding author address: Weile Wang, Department of Geography and Environment, Boston University, 675 Commonwealth Ave., Boston, MA 02215.

E-mail address: wliwang@bu.edu

be followed by lower rainfall but higher temperatures during July through September. These results suggest that initially enhanced vegetation may deplete soil moisture faster than normal and thereby induce drier and warmer climate anomalies via the strong soil moisture–precipitation coupling in these regions. Consistent with this soil moisture–precipitation feedback mechanism, interactions between temperature and precipitation anomalies in this region indicate that moister and cooler conditions are also related to increases in precipitation during the preceding months. Because vegetation responds to soil moisture variations, interactions between vegetation and precipitation generate oscillations in NDVI anomalies at growing season time scales, which are identified in the temporal and the spectral characteristics of the precipitation–NDVI system. Spectral analysis of the precipitation–NDVI system also indicates that 1) long-term interactions (i.e., interannual and longer time scales) between the two anomalies tend to enhance one another, 2) short-term interactions (less than 2 months) tend to damp one another, and 3) intermediary-period interactions (4–8 months) are oscillatory. Together, these results support the hypothesis that vegetation may influence summertime climate variability via the land–atmosphere hydrological cycles over these semiarid grasslands.

KEYWORDS: Land–atmosphere interaction; Vegetation feedbacks

1. Introduction

It is well known that terrestrial vegetation can influence climate through the exchange of energy, mass, and momentum between the land surface and the overlying atmosphere (Pielke et al. 1998). As a major pathway through which soil water is transferred into the atmosphere, vegetation generally promotes the land–atmosphere water exchange via evapotranspiration (Sellers et al. 1997; Gerten et al. 2004) and reduces surface temperatures by lowering the Bowen ratio (Bounoua et al. 2000). These mechanisms are illustrated by model simulations with extreme vegetation schemes (Fraedrich et al. 1999; Kleidon et al. 2000), which indicate that a green planet (100% vegetation coverage) has about 200% of the precipitation of a desert planet (0% vegetation coverage) and is about 8 K cooler than the latter.

However, the above description of vegetation feedbacks is a rather static view, referring to the mean status of the climate–vegetation system. Depending on specific regions and spatial–temporal scales under consideration, effects of vegetation on climate can be highly variable. For instance, as vegetation transfers water into the atmosphere, it can also lower soil water storage and dry the soil (Pielke et al. 1998). At the same time, the water vapor coming into the atmosphere may be transported out of the local air column, resulting in a net divergence of water flux from the region (e.g., Shukla and Mintz 1982). These processes may be particularly important for arid/semiarid regions, where soil water is limited and rainfall is infrequent. In the Midwest of the United States, for example, evapotranspiration exceeds precipitation during the summer months and leads to a net divergence of water (Shukla and Mintz 1982; Bonan and Stillwell-Soller 1998). In addition, the long memory of soil moisture may allow vegetation signals to persist for months before they begin to influence the atmosphere (Pielke et al. 1998). Such time-scale dependence further increases the complexity of interactions between vegetation and climate (see below).

The vast grasslands over midwestern North America (Figure 1; hereafter North American Grasslands) represent a typical semiarid environment in the northern midlatitudes, where variations of vegetation are closely associated with soil moisture (e.g., Woodward 1987; Churkina and Running 1998). At the same time, climate model studies (e.g., Koster et al. 2004) have suggested this region is one of the “hot spots” where soil moisture and precipitation are most tightly coupled during summer. Given vegetation’s control on the water cycle, this coupling also implies a strong coupling between vegetation and climate variations (Delire et al. 2004).

Satellite estimates of vegetation [e.g., the normalized difference vegetation index (NDVI; e.g., Myneni et al. 1998)] may provide an opportunity to detect the presumed land surface feedbacks upon observed precipitation and temperature variability over these grasslands. However, identifying the weak effects of vegetation on climate variability remains a difficult task for observational studies. Measurements of vegetation (e.g., NDVI), temperature, and precipitation are the *consequences* of the coupled climate–vegetation system, while the corresponding

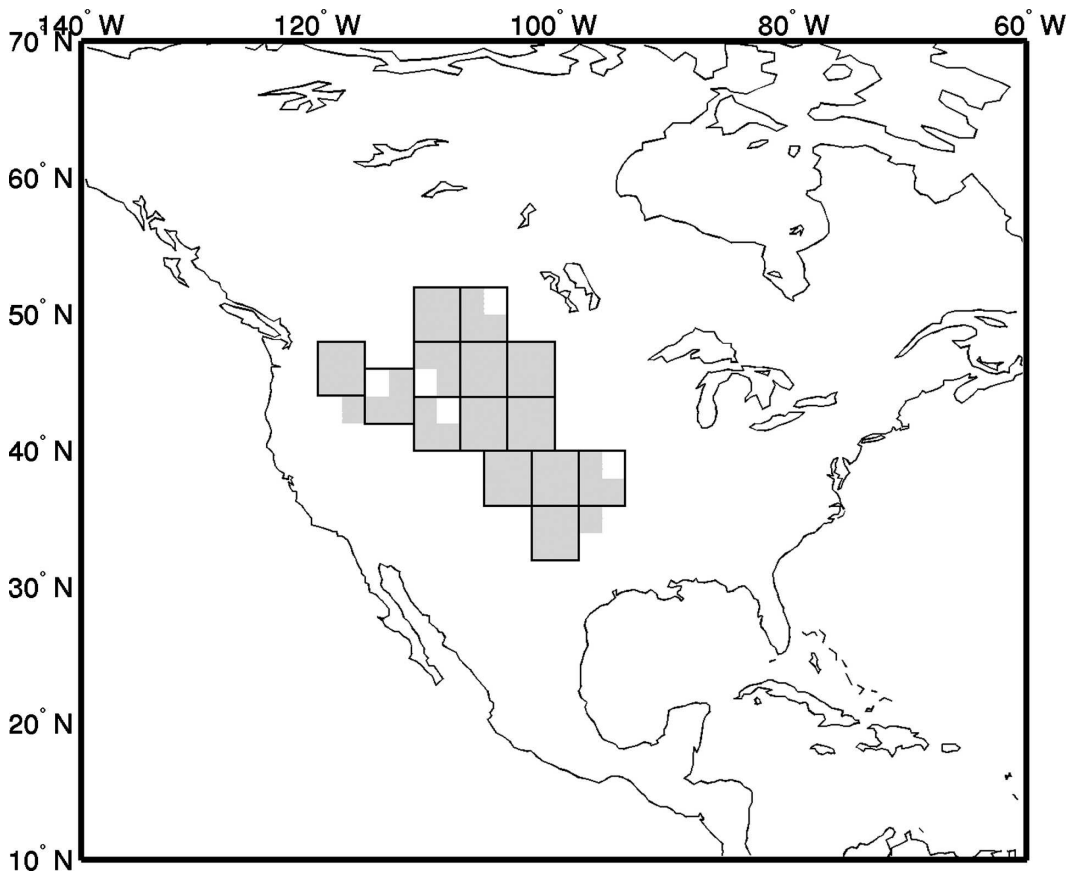


Figure 1. Domain of this analysis: the North American Grasslands. Shaded region shows 2° × 2° pixels of Grasslands as aggregated from the land cover map of Friedl et al. (Friedl et al. 2002), and the black grids indicate the 4° × 4° boxes that are used to resample the data.

controls remain unknown. For instance, it is difficult to use simultaneous observations (i.e., observed at the same time) to separate the portion of precipitation variability that constitutes the “original” climate signal from the portion that is induced by feedbacks from vegetation. Therefore, detection of causal relationships (i.e., forcing and feedbacks) from observations relies on the idea of predictability, that is, how much variance in precipitation (or other climate variables) can be predicted *exclusively* by past values of vegetation. The term “exclusively” is emphasized because information about current precipitation can also be provided by past values of precipitation or temperature (as well as other variables); however, we want to ensure that the explanatory power is contributed by vegetation alone. In this sense, the conventional technique of lagged-correlation analysis cannot fully answer the question posed here. Instead, this paper uses another methodology, namely, Granger causality (Granger 1969; 1980). The notion of Granger causality was developed in studies of economic time series; nevertheless, because the methodology has mathematical and physical foundations, it also has desirable properties for identifying causal relationships in climate studies (e.g., Kaufmann and Stern 1997; Salvucci et al. 2002; Wang et al. 2004). The concept of Granger causality and the associated testing techniques are introduced further in the methodology section.

Overall, this study focuses on the North American Grasslands in order to investigate vegetation feedbacks on climate variability in a semiarid environment. In the first part of this study (this paper), we use statistical techniques to analyze 1) whether lagged vegetation (NDVI) anomalies “Granger cause” summertime climate variability, 2) what components of intraseasonal vegetation variations contribute to such causal relationships, and 3) how such vegetation variability may be related to precipitation and/or soil moisture. We also test for causal relationships between temperature and precipitation anomalies to examine whether they are compatible with the assumed soil moisture–atmosphere feedbacks in this region. As will be shown below, answers to these questions provide consistent and coherent evidence for a physical mechanism in which vegetation influences climate variability via its influence on the local hydrological cycling in the semiarid grasslands. This hypothesized mechanism provides a foundation to develop a physically meaningful stochastic model to further quantify the observed climate–vegetation interactions; it is presented in the second part of this study (Wang et al. 2006, hereafter W2).

2. Datasets and methodology

2.1. Datasets

The temperature dataset is from the National Aeronautics and Space Administration (NASA) Goddard Institute for Space Studies (GISS) surface temperature analysis (Hansen et al. 1999). The GISS dataset is produced from collections of meteorological station records [Global Historical Climatology Network (GHCN)], and it provides monthly temperature anomalies (relative to the 1951–80 climatology) with global coverage at a $2^\circ \times 2^\circ$ spatial resolution. The precipitation dataset is from the National Oceanic and Atmospheric Administration (NOAA) Climate Prediction Center (CPC) Merged Analysis of Precipitation (CMAP; Xie and Arkin

1997). The CMAP dataset is derived from surface gauge measurements, precipitation estimates from multiple satellite-based algorithms, and output of numerical model predictions. It is available monthly at a $2.5^\circ \times 2.5^\circ$ resolution and is reprojected to $2^\circ \times 2^\circ$ grids in this study. The NDVI dataset is derived from the NOAA Advanced Very High Resolution Radiometer (AVHRR) instruments by the Global Inventory Monitoring and Modeling Studies group (GIMMS; Tucker et al. 2005). This version of the GIMMS NDVI dataset is corrected through a series of preprocessing steps to alleviate known limitations of the AVHRR measurements induced by intersensor calibration, orbital drift, and atmospheric contamination (Vermote and Kaufman 1995; Los 1998; Pinzon et al. 2001). The influences of the remaining artifacts are expected to be negligible at intraseasonal time scales (Kaufmann et al. 2000), and values of NDVI are consistent with ground-based vegetation measures such as tree rings (Kaufmann et al. 2004). For this study, NDVI data are aggregated to $2^\circ \times 2^\circ$ grid points to match the resolution of the climate datasets. Because these datasets provide high-frequency (monthly) measurements of the climate–vegetation system with global coverage, they have been used to investigate issues related to climate–vegetation variability in many previous studies (e.g., Zhou et al. 2001; Zhou et al. 2003; Kaufmann et al. 2003; Lotsch et al. 2003).

For all datasets, only data over the North American Grasslands (Figure 1) and during the period of 1982–2000 are used. A land cover map derived from Friedl et al. (Friedl et al. 2002) is used to determine the study domain, which identifies about 51 grid points (boxes) that have the biome type of grasslands that lie within 25° – 55° N and 90° – 130° W (Figure 1, shaded area). For each of these grid points, monthly anomalies of all variables are calculated relative to their 1982–2000 climatologies (i.e., long-term mean seasonal cycles). (We emphasize that the analyses and the results of this study are based on anomalies of these variables; yet in places where this reference is clear, the term “anomalies” or “variations” may be omitted in order to avoid lengthy repeats.) Finally, in order to increase the size of the data sample and thus make it feasible to analyze climate–vegetation interactions month by month, these gridpoint time series are further compiled into two panels for the North American Grasslands. The first panel uses the full fifty-one $2^\circ \times 2^\circ$ grid points (Figure 1, shaded area), and the second panel consists of 14 grid points resampled from 14 groups of 2×2 adjacent points (Figure 1, $4^\circ \times 4^\circ$ grid cells). Both panels are used throughout the analyses; however, because the results obtained with them are qualitatively the same, for simplicity below we mainly discuss those obtained with data resampled from the $4^\circ \times 4^\circ$ grid cells.

2.2. Granger causality

We illustrate the use of Granger causality by describing the procedures used to test whether NDVI anomalies Granger cause precipitation variations. Because causal relationships cannot be determined by concurrent correlations between two (or more) fields, the idea of Granger causality is based on predictability (Granger 1980). To utilize past information of climate (temperature and precipitation) and vegetation (NDVI) to “predict” the variability of current precipitation, we use the following statistical model:

$$P_m^i = \alpha + \beta \times \text{Year} + \sum_{l=1}^s \gamma_{m,l} \times T_{m-l}^i + \sum_{l=1}^s \varphi_{m,l} \times P_{m-l}^i + \sum_{l=1}^s \lambda_{m,l} \times N_{m-l}^i + \varepsilon_m^i \quad (1)$$

where P , T , and N represent anomalies of precipitation, temperature, and NDVI, respectively; the subscript m indicates the calendar month of interest, and the superscript i is the index of grid points; l is the lagged month, and s is the maximum lag length; α , β , γ s, φ s, and λ s are regression coefficients, and they are assumed to be the same across grid points; ε represents the residuals (or errors) of the regression. The variable “Year” is included in Equation (1) to account for a possible trend in the variables (Kaufmann et al. 2003).

Equation (1) is usually referred to as the *unrestricted* model because it specifies the full set of available information about climate and vegetation. Generally, if the lagged NDVI anomalies in Equation (1) are necessary for estimating the variability of current precipitation, the regression coefficients (i.e., λ s) associated with them will be distinct from zero. However, if lagged NDVI anomalies do not have information about current precipitation variations, or the information contained in NDVI anomalies is already contained in the lagged values of temperature and precipitation (i.e., the information is redundant), the values of λ s can be set to zero without reducing the explanatory power of the statistical model. In the latter case, Equation (1) can be written as

$$P_m^i = \alpha' + \beta' \times \text{Year} + \sum_{l=1}^s \gamma'_{m,l} \times T_{m-l}^i + \sum_{l=1}^s \varphi'_{m,l} \times P_{m-l}^i + \varepsilon_m'^i \quad (2)$$

Because the lagged values of vegetation are excluded from the information set, Equation (2) is called the *restricted* model.

Given the above logic, a test of whether lagged NDVI anomalies Granger cause current precipitation variations is to compare how estimates of current precipitation by the restricted model [Equation (2)] differ from estimates by the unrestricted model [Equation (1)]. A statistically significant ($p < 0.05$) reduction in the explanatory power (measured by the residual sum of squares, e.g.) of the restricted model suggests a causal relationship from NDVI to precipitation. In other words, NDVI Granger causes precipitation variability only if past values of NDVI anomalies contain statistically meaningful information about current precipitation variations that are not provided by other variables in the information set [i.e., past values of precipitation and temperature in Equation (1)].

Two methods are utilized to test for Granger causality in this study. The first method uses ordinary least squares (OLS) to estimate Equations (1) and (2) and tests NDVI’s causal relationship with precipitation using a partial F test. The second method tests the presence of Granger causality by examining the accuracy of out-of-sample forecasts (Granger and Huang 1997) generated by the unrestricted model [Equation (1)] against those generated by the restricted model [Equation (2)]. Briefly speaking, this method makes out-of-sample forecasts by using the statistical model to predict the climate–vegetation variability at grid points that are *not* used to retrieve model coefficients. As such, it can limit spurious fits of the statistical models to the panel data (Granger and Huang 1997).

For simplicity, we leave the details of both methods for appendix A. As described below, conclusions about the presence of a causal relationship generally are consistent across methods in this study.

The above example of whether vegetation “causes” precipitation variability can be easily extended to test causal relationships between other pairs of variables. For instance, a set of unrestricted and restricted equations that specify temperature as the dependent variable can be used to test for a causal relationship from NDVI to temperature anomalies. In the same way, we can also test relationships between temperature and precipitation anomalies. [Note that the causal influence of climate variables (precipitation, in particular) on vegetation over the semiarid grasslands will not be discussed in this paper because it is well studied in the literature (e.g., Woodward 1987) and is simply confirmed by our algorithm.]

Several issues about the Granger causality algorithm may need further clarification. The first is about the choice of the lag length (s) in the statistical models [Equations (1) and (2)]. Roughly, this parameter determines how much of the previous climate–vegetation variability is included in the statistical model to predict its future development. A large s includes more information (i.e., more lagged terms) in the models and thus may increase their explanatory power of the model. However, a large s also increases the number of regression coefficients and reduces the degrees of freedom of the analysis and hence the statistical significance of the results. Therefore, empirical approaches to determine s generally balance between these two considerations (Enders 1995). To reduce the sensitivity of the analysis to a specific time lag, in this study we repeat the test of Granger causality using time lags of 1–5 months. This range of time lags allows the seasonal evolution of vegetation (and soil moisture) to be included in the analysis (see below).

In addition, it is recognized that interactions between climate and vegetation are nonlinear in nature; however, in the statistical models [Equations (1) and (2)] these relationships are described through linear specifications. This simplification is based on the consideration that anomalies of climate/vegetation variables represent small deviations from their steady states, and thus their relationships may be linearly approximated (Glendinning 1994). Such an anomaly-based approach is commonly used in previous studies of the climate–vegetation system (e.g., Zhou et al. 2001; Zhou et al. 2003; Kaufmann et al. 2003) as well as ocean–atmosphere interactions (e.g., Czaja and Frankignoul 1999; Czaja and Frankignoul 2002). In addition, we provide a more detailed mathematical derivation of linearization of vegetation–climate interactions for anomalous data in the appendix of the companion paper (W2).

Finally, we recognize that the detection of Granger causality is limited by the specifications of the statistical model and the quality of the datasets. For example, the unrestricted model [Equation (1)] includes only information of temperature, precipitation, and NDVI, while observations of other important variables (e.g., soil moisture, cloudiness, and so on) are not available at the same spatial and temporal scales. As a result, the detection of Granger causality does not necessarily imply that a direct physical mechanism exists between the causal variable and the dependent variable. The actual causal relationship may be driven by a process that is missing from the information set (e.g., soil moisture). Furthermore, conclusions about Granger causality also can be influenced by the frequency or time scales of

the sample data (Wang et al. 2004). Therefore, caution is required in interpreting the statistical results in a physically meaningful way. Nevertheless, we hope to show that the method of Granger causality provides guidance in understanding the interactions within the highly coupled climate–vegetation system.

3. Results and discussion

3.1. Granger causality analysis

We test Granger causal order from NDVI to precipitation and temperature during the growing season with time lags [s in Equation (1)] from 1 to 5 months. Results consistently indicate a causal relationship when s is longer than 2 months. For simplicity, we discuss only the results obtained for s equal to 4 months; similar results are found when s is set to 3 or 5 months.

With a 4-month lag, the analysis focuses on the period from July to October. For these months, about 15%–20% of precipitation’s variance is captured by the unrestricted model (Figure 2a, white bars). The explained portion of the variance of temperature is generally about 20%–30%, but reaches 50% in August (Figure 2b,

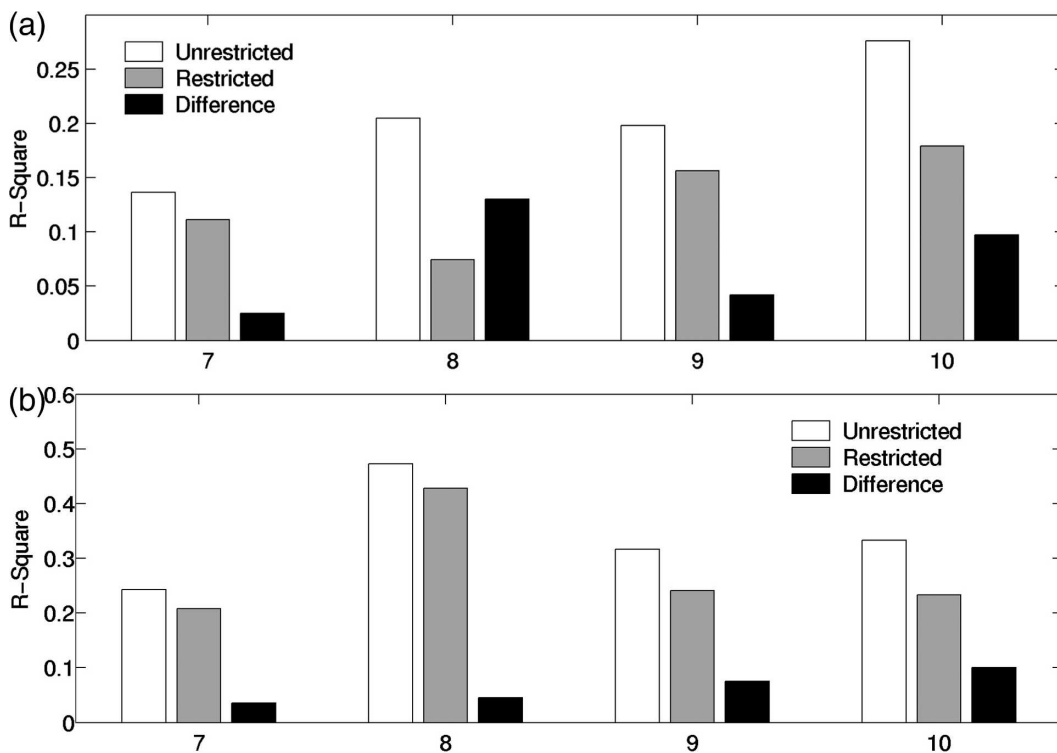


Figure 2. The performance (in terms of r^2) of the statistical models used to predict (a) precipitation and (b) temperature in July–October. The bars show the r^2 of 1) the unrestricted model (white), i.e., when the full information set is used; 2) the unrestricted model (gray), i.e., when NDVI is excluded from the model; and 3) the difference of r^2 between 1) and 2), which represents the explanatory power uniquely provided by NDVI (black).

white bars). For both precipitation and temperature, NDVI alone accounts for about 5% of the variance (Figures 2a,b, dark bars). Importantly, this contribution of explanatory power by NDVI is significant in a statistical fashion, as indicated by multiple testing metrics (Table 1). These results suggest that lagged NDVI anomalies have a statistically measurable effect on precipitation and temperature variability during all four months, with the exception of NDVI’s influence on July precipitation (Table 1).

Because the time lag is long (4 months) and there are correlations (i.e., col-linearity) among the lagged vegetation anomalies themselves, it is difficult to determine the nature of the causal relationships directly from the four regression coefficients associated with NDVI anomalies. Therefore, we try to identify the major intraseasonal modes of vegetation variability and determine their contributions to the causal relationship. For this purpose, we use the algorithm of empirical orthogonal functions [EOFs; also called principal component analysis (PCA); Kutzbach 1967; Bretherton et al. 1992] to decompose the 4-month evolution of NDVI during each year and at each grid point into four characteristic EOF components representing different modes of intraseasonal evolution; it is important to note that unlike traditional EOF analysis, we are not identifying spatial patterns that show similar time evolution but instead are identifying intraseasonal evolution patterns that are prevalent across grid points and across years. Each of these NDVI components is a weighted combination of monthly NDVI time series over the lagged period, with the weights (or loadings) determined by the EOF algorithm (Kutzbach 1967). The EOF components are ordered such that the first component accounts for the largest portion of the total intraseasonal variance, the second component accounts for the second-largest portion of the total variance, and so on. For this application, the first two EOF components explain more than 75% of the intraseasonal variance in the lagged NDVI anomalies.

Although EOFs do not necessarily relate to physical modes of spatiotemporal variability (e.g., Richman 1986), the weights for the two shown here (Figure 3) suggest that they are associated with certain physical characteristics. The first component has roughly the same weights for the four lagged months (Figure 3a);

Table 1. Results of Granger causality tests using the OLS method (the ω statistic) and the method of out-of-sample forecast (the $S_{2\alpha}$ and the $S_{3\alpha}$ statistics). Values in boldface or italics indicate that the results are significant at the 95% ($p < 0.05$) or 90% ($p < 0.10$) level, respectively. The signs associated with the $S_{2\alpha}$ and the $S_{3\alpha}$ statistics do *not* indicate the sign of the causal relationship. See appendix A for a detailed description about these statistics.

	Jul	Aug	Sep	Oct
(a) NDVI Granger causes precipitation				
ω	1.58	9.00	2.87	7.38
$S_{2\alpha}$	1.10	-2.08	-1.60	-2.08
$S_{3\alpha}$	0.58	-1.76	<i>-1.36</i>	-2.12
(b) NDVI Granger causes temperature				
	Jul	Aug	Sep	Oct
ω	2.54	4.66	6.03	8.26
$S_{2\alpha}$	<i>-1.35</i>	-2.08	<i>-0.98</i>	-1.96
$S_{3\alpha}$	<i>-0.84</i>	-2.07	-1.76	<i>-1.53</i>

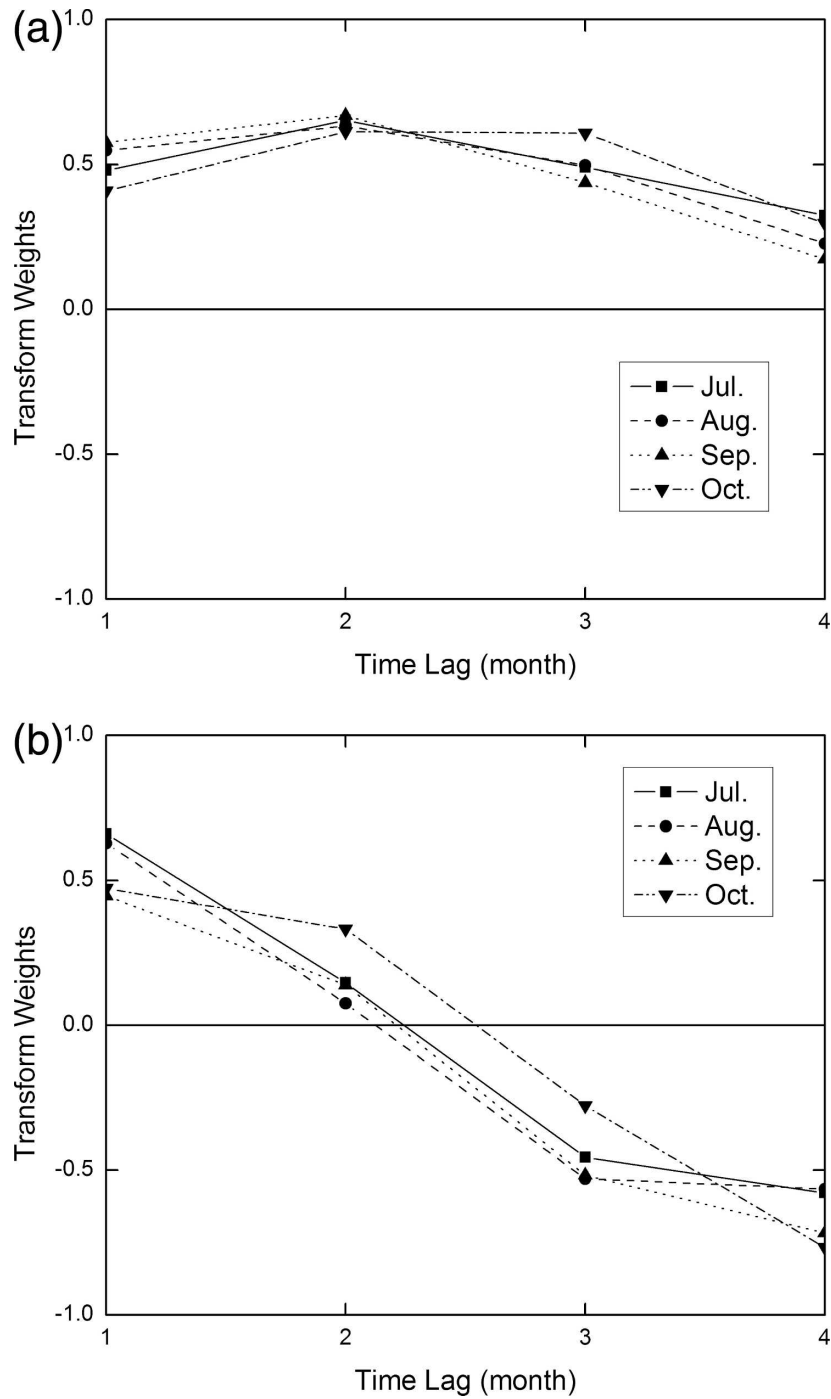


Figure 3. Weights for the first two EOF components of lagged NDVI anomalies for July–October. The calendar month (i.e., July, August, etc.) represents the *current* month that the respective lagged 4-month period is related to. For July, for example, a 1-month lag is related to anomalies in June. The first two components generally account for >75% of the intraseasonal variance of NDVI anomalies over the lagged period.

on the other hand, the weights of the second component are positive for the first two lagged months but are negative for the third and the fourth lagged months (Figure 3b). As such, these two components essentially represent the *mean* (denoted as \bar{N}) and the intraseasonal *trend* (denoted as N') of the lagged NDVI anomalies, respectively. To avoid using the specific weights from the EOF analysis, which can be sensitive to the number of grid points and time series used, we formulize these two intraseasonal characteristics as follows:

$$\bar{N} = \sum_{l=1}^4 \text{NDVI}_{m-l}/4,$$

$$N' = \sum_{l=1}^2 \text{NDVI}_{m-l}/2 - \sum_{l=3}^4 \text{NDVI}_{m-l}/2, \tag{3}$$

where m indicates the current month and l is the time lag.

We repeat the Granger causality tests with lagged NDVI terms in Equation (1) represented by \bar{N} and N' . As before, regression results indicate a causal relationship from NDVI to climate variability from July through October; in particular, both \bar{N} and N' significantly contribute to this causal relationship (Table 2). The signs of the regression coefficients associated with them (Table 2) indicate that 1) during July through September, the causal relationship from \bar{N} to precipitation anomalies is generally negative, while the relationship from \bar{N} to temperature anomalies is positive; 2) at the same time, the causal relationship from N' to precipitation anomalies is positive, and the relationship from N' to temperature anomalies is negative; and 3) in October, \bar{N} has a negative causal relationship with both precipitation and temperature anomalies; also, the relationship from N' to precipitation becomes negative in October (Table 2).

The statistical causal relationships in Table 2 can be interpreted as follows: 1) higher mean NDVI anomalies (\bar{N}) from the preceding months tend to be followed by lower rainfall and higher temperature during July through September; 2) if NDVI anomalies (N') show a decreasing trend, the following summer months are also likely to be drier and warmer; and 3) for October, however, higher NDVI seems to reduce both rainfall and temperature. (Appendix B provides another interpretation for the results of Table 2. Both interpretations, however, agree with one another in suggesting that higher NDVI anomalies earlier in the growing season may have negative impacts on precipitation variability in late summer.)

Table 2. OLS regression coefficients associated with the two major NDVI components, \bar{N} and N' (Equation (3)). Values in boldface or italics indicate that the results are significant at the 95% or 90% level, respectively.

	Jul	Aug	Sep	Oct
	(a) NDVI Granger causes precipitation			
\bar{N}	1.44	-6.99	<i>-3.54</i>	-2.19
N'	4.44	2.47	2.29	-4.45
	(b) NDVI Granger causes temperature			
	Jul	Aug	Sep	Oct
\bar{N}	6.85	8.05	8.56	-5.96
N'	-4.55	-2.11	-6.13	0.30

The preceding results may appear to disagree with the common assumption that in a semiarid environment, higher vegetation anomalies are associated with higher soil moisture (e.g., Woodward 1987) and are thus related to enhanced rainfall (e.g., Koster et al. 2004). To reconcile such apparent discrepancies, however, we should first emphasize the time scales in this analysis. The results of Table 2 suggest that positive vegetation anomalies *earlier in the growing season* may induce lower rainfall *later in summer* (July–September). As will be shown later, enhanced vegetation early in the season does not necessarily indicate higher vegetation anomalies several months later, nor does moist soil in spring always imply a water surplus in summer. Instead, if we assume a link between initially enhanced vegetation and lower soil moisture later in the season (see below), the results of Table 2 are self-consistent. They suggest that higher NDVI anomalies earlier in the growing season may generate drier soil later in summer, which in turn induces drier and warmer climate anomalies (Table 2, the first set of results associated with \bar{N}). At the same time, because vegetation tends to decrease in response to drier soil, decreasing trends of vegetation anomalies are also likely a precursor of reduced precipitation and increased surface temperature (Table 2, the second set of results associated with N'). These explanations present a starting hypothesis for the vegetation feedbacks detected by the Granger causality algorithm, which we now wish to develop and verify.

3.2. Seasonal oscillations of NDVI anomalies

An important consequence that follows from the above hypothesized chain of processes is that higher vegetation anomalies will tend to be followed by lower precipitation anomalies (and vice versa for the opposite-sign anomalies). Coupled with the known positive relationship between precipitation and subsequent vegetation anomalies, these interactions suggest an oscillatory variability of NDVI, which we examine in different ways.

First, we calculate autocorrelations of NDVI anomalies for each month between July and October (Figure 4). For example, the autocorrelation of October with a 5-month lag is the correlation between NDVI anomalies in October and those in May. Overall, autocorrelations of NDVI decrease as the time lag increases (Figure 4). For all months, autocorrelations are about 0.7 at the first lagged month (Figure 4), which suggests that vegetation anomalies are relatively persistent. However, as the time lag increases to about 3 months, these autocorrelations start to become negative (Figure 4). The negative autocorrelations are about -0.2 (significant at the 95% level) after 4 months or longer (Figure 4), which indicates that higher (lower) NDVI values early in the spring are likely followed by lower (higher) values later in summer. Together, the positive autocorrelations at shorter time lags and negative autocorrelations at longer time lags suggest that NDVI anomalies may oscillate (around their climatological values) over the course of a growing season (Enders 1995).

To visualize such oscillations and examine how they are related to climate variability, we compile indices of monthly NDVI anomalies and seasonal mean precipitation anomalies by averaging the gridpoint time series over the North American Grasslands (Figure 5). The mean precipitation anomalies are averaged from the beginning of the year to the end of the growing season, and therefore

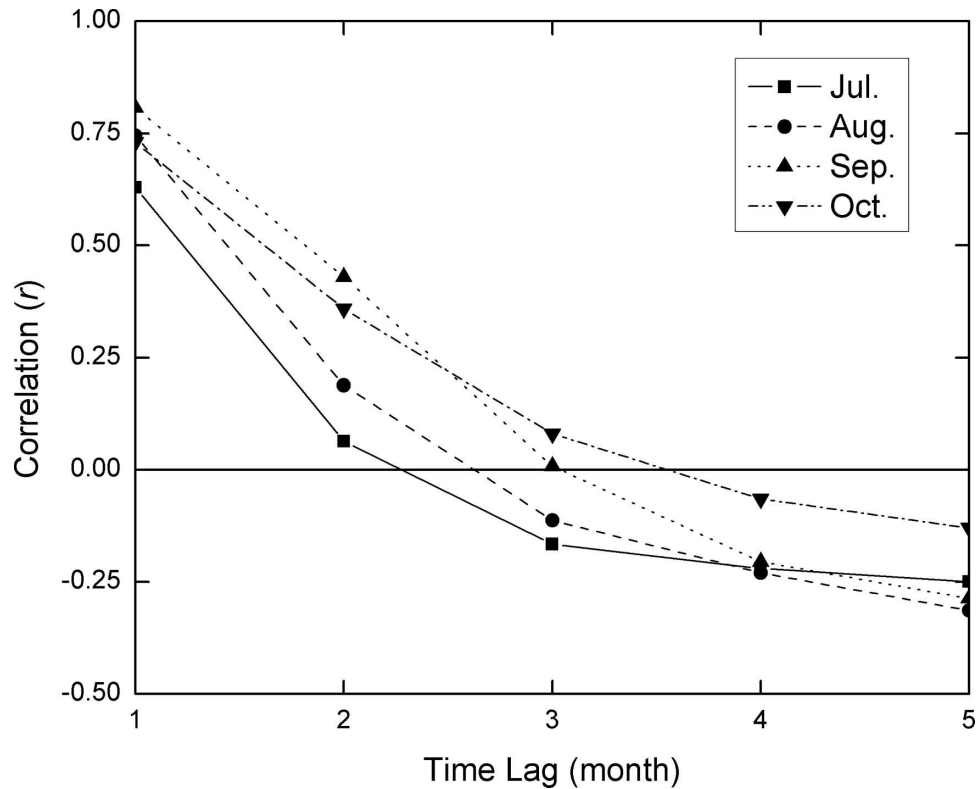


Figure 4. Autocorrelation of NDVI for the months of July–October. The maximum lag length is 5 months. The calendar month (i.e., July, August, etc.) represents the *current* month that the respective lagged 4-month period is related to. The 95% critical value for these autocorrelations is about ± 0.13 .

serve as a qualitative proxy for soil wetness through the season. As shown, the NDVI index apparently has an oscillatory component at growing season time scales (Figure 5a), whose evolution appears related to the *seasonal* mean soil wetness: in wet years (e.g., 1993), NDVI generally increases first and then decreases (producing a “dome” shape); in contrast, in dry years (e.g., 1988), NDVI often decreases first and then increases (producing a “U” shape).

To further illustrate this feature, we compile monthly NDVI and precipitation anomalies from all wet years (i.e., years with positive seasonal mean precipitation anomalies) to form a growing season composite (the “wet” composite; Figure 5b). For these wet years, the average NDVI starts at slightly negative values in April and May, reaches its peak in July and August, and then decreases again in September and October (Figure 5b). The trajectory of the NDVI composite clearly shows a dome shape (Figure 5b). Because the NDVI anomalies are calculated relative to their climatologies for the observation period, the composite for the dry years is just the same as Figure 5b but with the opposite sign (not shown).

The evolution of NDVI and precipitation indices in Figure 5b offer a qualitative explanation for the oscillatory adjustments of vegetation anomalies and how they may feed back to precipitation. If we assume that the mean values of the

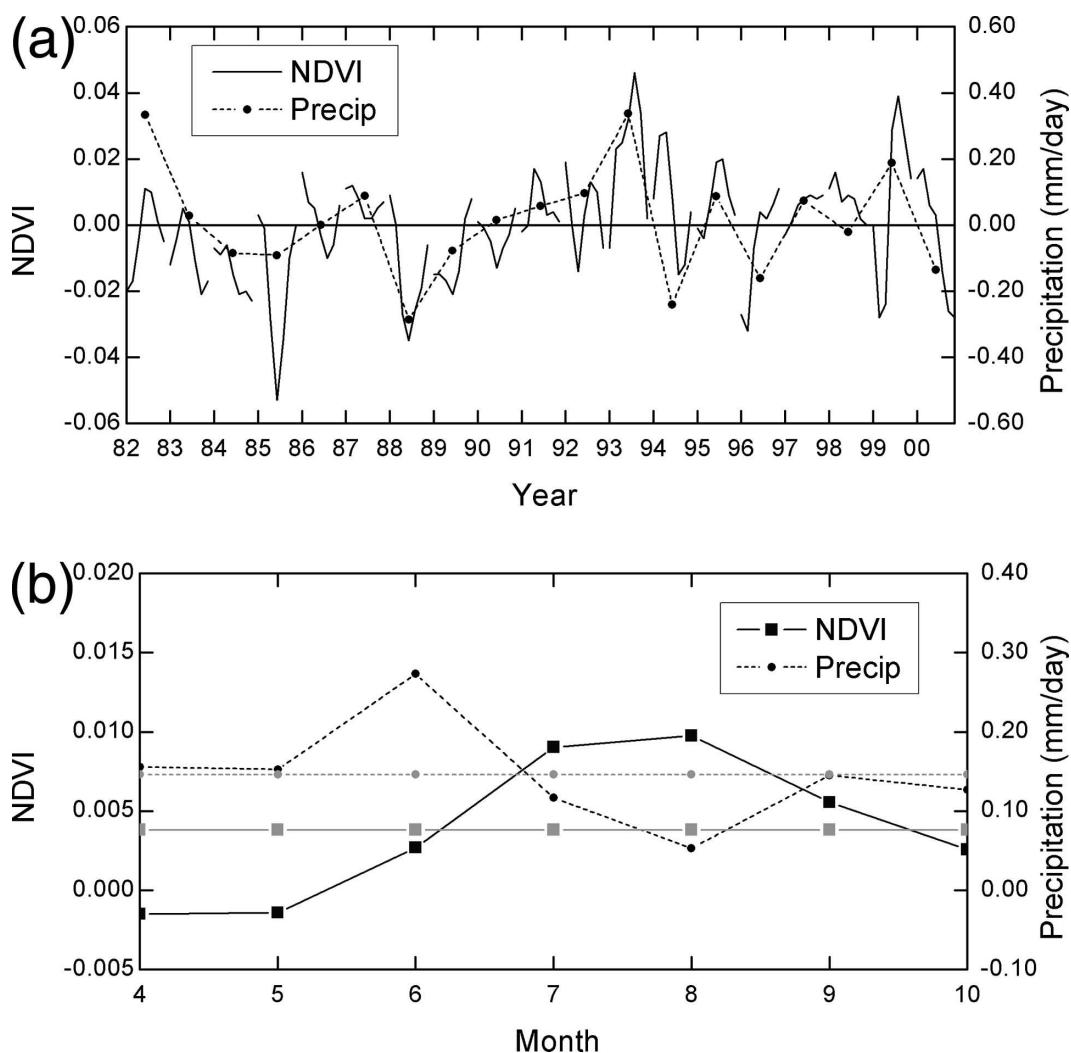


Figure 5. (a) Indices of monthly NDVI anomalies and seasonal mean precipitation anomalies (averaged over January–October for the given year). Monthly values of NDVI only shown for the period April–October; (b) Growing season composites of monthly NDVI and precipitation anomalies for years in which the seasonal-mean precipitation anomalies are positive (the wet composites). The two light gray lines show the seasonal mean anomalies of NDVI and precipitation, respectively. The corresponding “dry” composites are the same as the wet composites but with the opposite signs.

composites of NDVI and precipitation anomalies tend toward a climatological equilibrium, when precipitation (and hence soil moisture) is initially in surplus (April), vegetation will tend to grow (Figure 5b). However, as NDVI increases beyond its equilibrium with precipitation (e.g., in July and August), soil moisture will change from a water surplus to water deficit, which in turn moves NDVI back to its seasonal mean value in September and October (Figure 5b). For precipitation, the positive anomalies in June shrink as the vegetation anomalies become

positive and produce an excess draw-down of soil moisture. Precipitation anomalies continue to decline through the growing season when the NDVI anomalies are high and then start to increase again as the NDVI values begin to decrease (Figure 5b). While it is expected that vegetation would respond to variations in the precipitation field, if precipitation were purely a stochastic phenomenon on time scales longer than a few days, there would not necessarily be a strong intraseasonal structure to its behavior when composited on seasonal-mean values. Hence the apparent oscillatory component of precipitation over the course of the season may reflect interactions with vegetation-mediated soil moisture.

The relationship between the oscillatory components of NDVI and precipitation anomalies can be quantitatively examined by the spectral characteristics of the precipitation–vegetation system. If we assume that NDVI anomalies are driven solely by precipitation variations, the frequency response functions of the system (the gain function and phase function; Figure 6) can be estimated from the relationship between NDVI anomalies (output) and precipitation anomalies (input) in the Fourier spectral domain using the methodology described in Jenkins and Watts (Jenkins and Watts 1968). Simply speaking, we first calculate the Fourier spectra of vegetation and precipitation anomalies over every growing season and then estimate the correlation coefficients between the spectra of vegetation and precipitation at different frequencies (or periods). Because these correlation coefficients

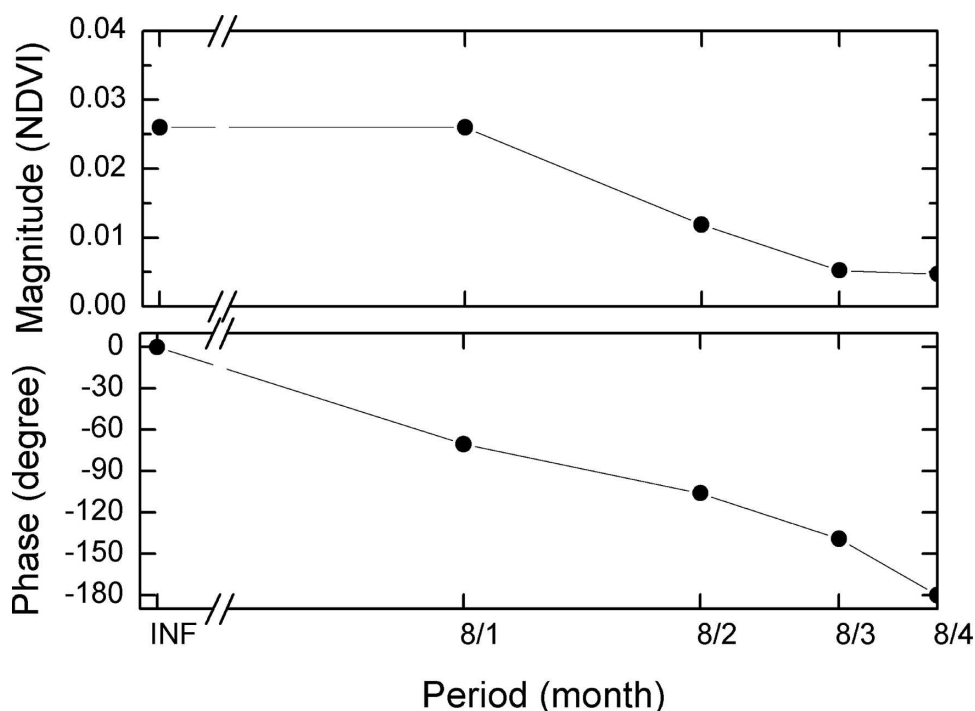


Figure 6. (top) The gain function and (bottom) the phase function of the precipitation–NDVI system, estimated based on FFT spectra of growing season anomalies (April–October; 7 months). The magnitude of the gain function is in units of NDVI per unit precipitation (mm day^{-1}).

cients have complex values in general, they contain both magnitude (i.e., the gain function) and phase relationships between the two fields.

The estimated gain function (Figure 6, top) indicates that the responses of NDVI anomalies to precipitation forcing are stronger at the 8-month period and at the climatological time scale, where the magnitudes are about 5 times as high as at the 2-month period. Such “red” responses suggest that NDVI anomalies will have a strong response component at growing season time scales (as observed in Figure 5), even when they are driven by “white-noise” precipitation. In addition to the gain function, the phase function (Figure 6, bottom) shows that NDVI anomalies are in phase with precipitation forcing at long time scales (e.g., the constant component); however, vegetation signals lag behind precipitation as the frequency increases. The phase lags at periods of 8, 4, and 2 months are about 75° , 90° , and 180° , respectively (Figure 6, bottom).

The spectral analysis approach also provides a better understanding of how vegetation’s influence on precipitation may change with the time scales considered. At long time scales (e.g., interannual or longer scales), when NDVI varies in phase with precipitation (Figure 6, bottom) and has higher magnitudes (Figure 6, top), it is expected that vegetation feedbacks will enhance precipitation, resulting in a positive feedback between the two. At high frequencies (e.g., at 2-month periods), when NDVI varies in the opposite direction of precipitation (phase lag of 180°), vegetation will tend to damp the variability of the precipitation forcing, resulting in a negative feedback between the two. At intermediate time scales (e.g., periods of 4–8 months), because the phase lag is about 90° (Figure 6, bottom), feedbacks of NDVI will produce oscillatory behavior in the precipitation signal in which initially enhanced vegetation, related to enhanced precipitation, is followed by reduced rainfall several months later, as indicated by the Granger causal relationship analysis (Table 2).

3.3. Soil moisture–precipitation coupling

Above we have assumed a positive relationship between soil moisture and precipitation over the study region, which has been suggested by climate model studies (e.g., Shukla and Mintz 1982; Bonan and Stillwell-Soller 1998; Pal and Eltahir 2001; Koster et al. 2004). This assumption can be tested indirectly by examining how precipitation variability is related to *climate* anomalies (i.e., temperature and precipitation) from the preceding months. If there is a relationship between positive soil moisture anomalies and enhanced rainfall, it is expected that excess rainfall early in the season will increase soil moisture and therefore have a positive relationship with its own variations later in the season. At the same time, it is also expected that positive temperature anomalies early in the season will enhance evaporation and decrease local soil moisture, which will reduce precipitation later in the season.

We use the Granger causality algorithm to test the above hypothesis.¹ The results generally indicate statistically measurable causal relationships from lagged

¹ Here by saying that lagged precipitation anomalies Granger causes current precipitation variability, we simply mean that the former contains information about the latter that is not provided by other lagged variables (e.g., temperature and vegetation) as discussed above.

anomalies of precipitation and temperature to current precipitation variability (Table 3, for time lags of 2 months). The nature of these relationships is given by the signs of the regression coefficients associated with the mean precipitation/temperature anomalies over the lagged period. Generally, the causal relationship from lagged precipitation to current precipitation variability is positive, and the relationship from lagged temperature to current precipitation variability is negative during summer but positive at the beginning and the end of the growing season (Table 3).

The nature of the above causal relationships is further illustrated by the corresponding lagged correlations (Figure 7). Overall, correlations between current precipitation and its preceding mean anomalies are positive (about 0.15 on average) through the year (Figure 7a), although there are two major troughs in April–May and October when the correlations drop below zero, and a minor trough in July when the correlations become trivial (Figure 7a). On the other hand, correlations between current precipitation anomalies and the preceding mean temperature anomalies are negative (about –0.13) during May through September, but positive (about 0.14) in the other months, with the only exception in December (Figure 7b).

Together, Table 3 and Figure 7 indicate that in summer precipitation anomalies have a positive relationship with their previous variations, while the relationships between precipitation and the preceding temperature anomalies are negative. These results are consistent with the soil moisture–precipitation feedback described earlier and with other previous studies (e.g., Trenberth and Shea 2005; Zeng et al. 2005). It is also noted that there is a switch of the sign related to temperature’s effect on precipitation in winter and early spring, when temperature anomalies have positive correlations with precipitation variations in the following months (Figure 7b). It is possible that during these times of year higher temperatures may increase the atmosphere’s capacity to hold more moisture and thus lead

Table 3. Granger causal relationships from lagged anomalies of (a) temperature and (b) precipitation to current precipitation variability. Results shown are calculated with 2-month time lags. The sign of the relationship is determined from the regression coefficients associated with the mean temperature/precipitation anomalies over the lagged period. The statistics of ω , $S_{2\sigma}$, and $S_{3\sigma}$ are the same as in Table 1. Values in boldface or italics indicate that the results are significant at the 95% or 90% level, respectively.

	Mar	Apr	May	Jun	Jul	Aug	Sep	Oct
(a) Temperature Granger causes precipitation								
Sign	+	+	–	–	–	–	+	+
Ω	4.51	5.58	2.68	0.64	2.38	1.37	0.79	7.59
$S_{2\sigma}$	-1.59	-0.70	-2.61	-2.74	<i>-1.34</i>	-0.32	-0.95	-2.86
$S_{3\sigma}$	-1.83	-0.48	-2.46	-2.08	<i>-1.22</i>	0.44	-1.73	-2.45
(b) Precipitation Granger causes precipitation								
	Mar	Apr	May	Jun	Jul	Aug	Sep	Oct
Sign	+	+	–	+	–	+	+	–
Ω	9.76	1.33	2.40	5.11	0.01	0.06	2.03	3.78
$S_{2\sigma}$	<i>-1.21</i>	-0.19	-0.83	<i>-1.59</i>	2.48	-2.61	-0.83	-1.72
$S_{3\sigma}$	-1.79	-0.03	-0.36	<i>-1.22</i>	2.34	-2.05	-0.73	-1.85

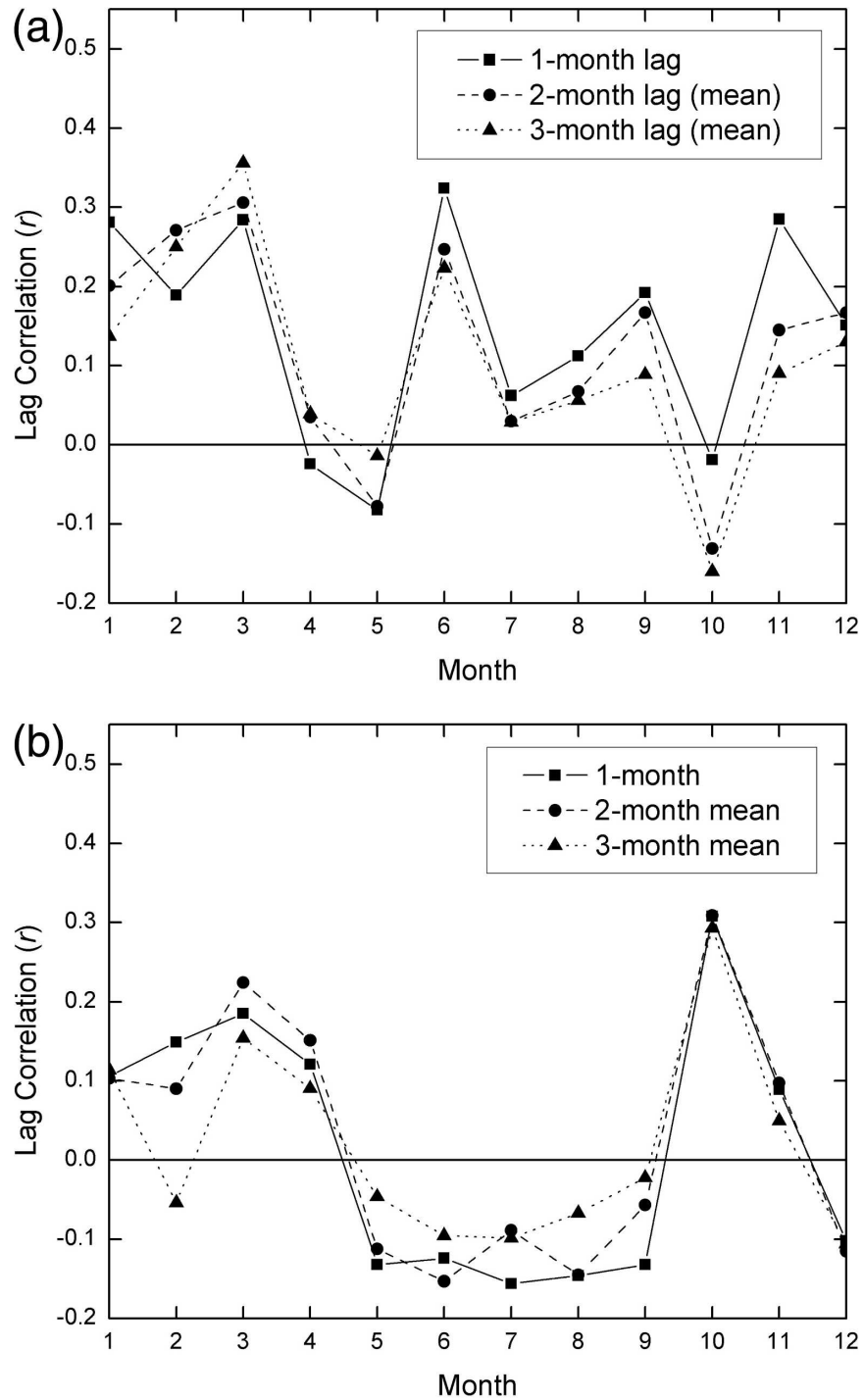


Figure 7. Lagged correlations (r) between current precipitation anomalies and mean anomalies of (a) precipitation and (b) temperature from the preceding 1–3 months. The abscissa (“month”) indicates the current calendar month. The 95% and the 90% critical values for these correlations are about ± 0.13 and ± 0.10 , respectively.

to higher precipitation (Trenberth and Shea 2005); further investigation of this relation, however, is beyond the scope of this paper.

3.4. Discussion of physical hypothesis

The results presented in this paper, although only based on statistical analysis, allow us to propose a physical mechanism for land–atmosphere interactions over the North American Grasslands. In particular, we argue that higher vegetation anomalies at the beginning of the growing season may reduce soil moisture faster than normal and initiate drought conditions later in summer, which in turn reduces vegetation productivity. The negative relationship between the seasonal mean vegetation anomalies (\bar{N}) and precipitation variations (Table 2) is in agreement with this hypothesis; the positive relationship between the seasonal trend in vegetation anomalies (N') and precipitation variations (Table 2) is also consistent with this hypothesis. The oscillatory variations in vegetation, which are captured by the autocorrelation analysis (Figure 4), the composite plots (Figure 5), and the spectral analysis (Figure 6), further support the proposed interactions of vegetation with soil moisture. Finally, the causal relationship between temperature and precipitation (Table 3) is consistent with the implied role of soil moisture in mediating the land–atmosphere exchanges of moisture and energy in this region. Together, all of these findings strongly suggest that vegetation, through its impact upon soil moisture, can modulate local climate.

The validity of the mechanism proposed here will be further assessed in the companion paper (W2). To give a brief description, W2 constructs and analyzes a stochastic model in which vegetation and precipitation interact via soil moisture to produce damped, enhanced, and oscillatory behavior of the vegetation–climate system at time scales similar to those found in the observations. It details the climatological parameters that generate the oscillatory behavior (compared to a stable, damped evolution). Furthermore, W2 shows that only when feedbacks of vegetation upon soil moisture and precipitation are included in the stochastic model can it properly simulate the observed Granger causality. This latter result suggests that the observed vegetation–climate interactions analyzed in this paper are not an artifact of the statistical analysis itself.

Now we want to further discuss how this proposed mechanism, part of which has also been suggested by previous studies (e.g., Heck et al. 1999; Heck et al. 2001), relates to previous findings in the literature. While we recognize that the results of this study (based on monthly anomalies) may not be directly comparable to some of the studies that examine the steady state of the climate–vegetation system, these previous studies highlight *physical mechanisms* that link the climate and vegetation subsystems that may also be relevant on intraseasonal time scales.

First, the regulation of soil moisture on vegetation growth and the positive coupling between soil moisture and precipitation, as required by our proposed hypothesis, are well known (e.g., Woodward 1987; Churkina and Running 1998; Shukla and Mintz 1982; Koster et al. 2004). The negative effect of vegetation on soil moisture (i.e., the depletion effect) also can be inferred from the soil water budget, which is balanced by the input from precipitation and the loss through evapotranspiration and runoff (e.g., see Bonan 2002, chapter 5). For an arid/semiarid environment (e.g., the North American Grasslands), water loss through runoff is generally negligible (Feteke et al. 2000), and thus the balance of soil

moisture is largely maintained by precipitation and by evapotranspiration associated with vegetation (Wever et al. 2002). As such, the depletion of soil moisture by vegetation is known to become an important component of the hydrological cycle in semiarid regions (Montaldo et al. 2005), as argued here.

Second, the effects of vegetation upon precipitation suggested by our statistical results are also supported by coupled climate–vegetation model studies. For instance, Heck et al. (Heck et al. 1999; Heck et al. 2001) report that increasing vegetation in a regional climate model leads to moister and cooler spring conditions but drier and warmer summers in the Mediterranean region, which is explained by a similar mechanism as proposed above. Delire et al. (Delire et al. 2004) report that in the fully coupled National Center for Atmospheric Research (NCAR) Community Climate Model version 3 and the Integrated Biosphere Simulator (CCM3–IBIS) model simulations, dynamic vegetation cover tends to enhance the long-term (e.g., decadal or longer) variability of precipitation but damp it at shorter (e.g., interannual) time scales; in particular, such vegetation–precipitation interactions are most significant over ecological transition zones that include the North American Grasslands. Although mechanisms for the long-term vegetation–atmosphere interactions in the coupled CCM3–IBIS are different from (and much more complicated than) the intraseasonal interactions discussed in this paper, both studies are consistent in that they argue that the nature of vegetation feedbacks can change with various time scales.

Third, our results indicate that NDVI anomalies over the North American Grasslands contain a distinct oscillatory component during the course of a growing season. These results are in agreement with other studies (e.g., Wu et al. 2002) that report similar intraseasonal variability in root zone soil moisture over adjacent Illinois. In addition, from an ecological perspective, the conditions of life over these grasslands are known to be severe (Weaver 1954); as such the oscillatory behavior discussed here may be induced by the fact that plants may “overshoot” their equilibrium conditions in order to gain advantages in competing for available water, although this requires further investigation.

Finally, the hypothesized mechanism and the spectral analysis of this study are also consistent with literature indicating that vegetation feedbacks can enhance precipitation at long time scales (e.g., Fraedrich et al. 1999; Kleidon et al. 2000). Here we note, however, that such “positive” feedbacks between vegetation and precipitation are not directly indicated by the results of the Granger causality test (i.e., Table 2). This may be because the long-term positive feedback process requires a persistence of the precipitation anomalies, while the Granger causality algorithm is specifically designed to identify climate variation *not* found in the preceding values of the climate parameters themselves. Although the Granger causality test may not be an appropriate tool for analyzing long time-scale variations, the frequency response function analysis does indicate that similar long time-scale interactions exist in the observed system.

4. Summary

This paper analyzes feedbacks of vegetation on climate variability over the North American Grasslands. Results indicate that NDVI anomalies early in the growing season have statistically significant Granger causal relationships with

anomalies of precipitation and temperature in late summer (July–October). The nature of the relationship indicates that higher mean values and/or decreasing trends of NDVI anomalies from the preceding months may lead to (or Granger cause) lower rainfall but higher temperatures in July through September. Combined with the positive influence of precipitation–soil moisture on subsequent NDVI anomalies, these results suggest that interactions between vegetation and soil moisture may generate oscillations at intraseasonal time scales.

The oscillatory variability of NDVI anomalies and its association with precipitation is further analyzed in the frequency domain. Empirical estimates for system functions indicate that the magnitude of NDVI’s responses to precipitation forcing becomes higher toward lower frequencies, while the phase lag of NDVI (relative to precipitation) increases with frequency. Such frequency characteristics indicate that vegetation feedbacks enhance precipitation variability at lower frequencies, but have the opposite effect at higher frequencies, and will tend to produce oscillations at intermediary time scales.

Finally, to test whether the influence of NDVI variations on climate variability discussed above are consistent with the expected soil moisture–precipitation feedbacks identified by Koster et al. (Koster et al. 2004), causal relationships between anomalies of precipitation and temperature are examined. The variability of summer precipitation is positively related to its own anomalies over the preceding months but is negatively related with those of temperature, as expected for a semiarid region in which soil moisture plays an important intermediary role in constraining both the land–atmosphere energy and water exchanges (e.g., Trenberth and Shea 2005; Zeng et al. 2005). While these results are focused on the North American Grasslands, they may have broader implications for vegetation–climate interactions in other water-limited regions as well as for vegetated regions that become water stressed as a result of long-term, larger-scale climate changes.

Acknowledgments. This work was supported in part by the NASA Earth Science Enterprise. The views expressed herein are those of the authors and do not necessarily reflect the views of NASA. The authors are thankful to Dr. Guiling Wang and another anonymous reviewer for their constructive comments and suggestions. GISS temperature data were provided by the NASA GISS Surface Temperature Analysis from their Web site (<http://data.giss.nasa.gov/gistemp/>). CMAP precipitation data were provided by the NOAA–CIRES ESRL/PSD Climate Diagnostics branch, Boulder, Colorado, from their Web site (<http://www.cdc.noaa.gov/>). We also would like to thank Dr. C. J. Tucker for providing the GIMMS NDVI data.

Appendix A

Algorithms to Test Granger Causality

To facilitate discussion, Equations (1) and (2) are rewritten here as Equations (A1) and (A2):

$$P_m^i = \alpha + \beta \times \text{Year} + \sum_{l=1}^s \gamma_{m,l} \times T_{m-l}^i + \sum_{l=1}^s \varphi_{m,l} \times P_{m-l}^i + \sum_{l=1}^s \lambda_{m,l} \times N_{m-l}^i + \varepsilon_m^i \quad \text{and} \quad (\text{A1})$$

$$P_m^i = \alpha' + \beta' \times \text{Year} + \sum_{l=1}^s \gamma'_{m,l} \times T_{m-l}^i + \sum_{l=1}^s \varphi'_{m,l} \times P_{m-l}^i + \varepsilon_m^{i'} \quad (\text{A2})$$

1.1. Ordinary least squares

As discussed in the methods section, the null hypothesis here is that eliminating the lagged values of NDVI from Equation (A1) does not reduce its explanatory power in a statistically meaningful fashion. To test this hypothesis, a statistic is constructed as follows:

$$\omega = \frac{(\text{RSS}_r - \text{RSS}_u)/s}{\text{RSS}_u/(L - k)}, \quad (\text{A3})$$

where RSS represents the residual sum of squares, while the subscripts r and u refer to the “restricted” and the “unrestricted” model [i.e., Equations (A2) and (A1)], respectively; s is the number of coefficients restricted to zero in Equation (A2); L is the number of total observations (i.e., $L = 14 \times 19$); and k is the number of regressors in Equation (A1). The test statistic (ω) can be evaluated against an F distribution with s and $L - k$ degrees of freedom in the numerator and denominator, respectively. High values of ω that exceed the 5% threshold indicate that NDVI anomalies “Granger cause” precipitation variability.

1.2. Out-of-sample forecast

First, we use the following procedure to make out-of-sample forecasts for the observed precipitation variations:

- (i) Eliminate one box (e.g., j) from the panel, which subsequently decreases the size of the panel by 1 (i.e., $14 - 1$).
- (ii) Use data from the remaining boxes ($I = 1 - 14, i \neq j$) to estimate the regression coefficients for Equations (A1) and (A2), respectively.
- (iii) Use the regression coefficients estimated in (ii) to make a forecast for the box of j . The forecasts generated with Equations (A1) and (A2) are denoted as $\hat{P}_{m,U}^j$ and $\hat{P}_{m,R}^j$, respectively.
- (iv) Repeat the above processes for each of the boxes in the panel.

Next, we compare the accuracy of the two sets of out-of-sample forecasts, by the unrestricted model Equation (A1) and by the restricted model Equation (A2), using the following metric:

$$I_+(d_t) = \begin{cases} 1, & d_t > 0 \\ 0, & \text{otherwise} \end{cases} \quad (\text{A4})$$

where

$$d_t = [\text{Precip}_m^i - \hat{P}_{m,U}^i]^2 - [\text{Precip}_m^i - \hat{P}_{m,R}^i]^2. \quad (\text{A5})$$

To test the null hypothesis that the out-of-sample forecasts are statistically equivalent, two statistics (Diebold and Mariano 1995) are constructed as follows:

$$S_{2a} = \frac{\sum_{t=1}^L I_+(d_t) - 0.5L}{\sqrt{0.25L}}, \tag{A6}$$

$$S_{3a} = \frac{\sum_{t=1}^L I_+(d_t)\text{rank}(d_t) - L(L+1)/4}{\sqrt{L(L+1)(2L+1)/24}}, \tag{A7}$$

where L is the number of total observations (i.e., $L = 14 \times 19$). The S_{2a} and S_{3a} statistics can be evaluated against a Student's t distribution with degrees of freedom equal to $(L - 1)$. Note that if the forecast errors generated by the unrestricted model [Equation (A1)] are smaller than those of the restricted model [Equation (A2)], the test statistics will be *negative*. Therefore, only negative values of S_{2a} and S_{3a} that are lower than the 5% threshold (which itself is negative) indicate the presence of Granger causality.

Appendix B

Complementary Explanations for Table 2

In determining the major components of vegetation variability and their causal relationships with climate variations, we estimated the *mean* (denoted as \bar{N}) and the intraseasonal *trend* (denoted as N') of the lagged NDVI anomalies, respectively [Equation (3)]. However, it is noted that vegetation information contained in \bar{N} and N' can also be represented in other ways. For instance, if we define $N_{1,2}$ as the mean NDVI anomalies over the first two lagged months, and $N_{3,4}$ as the mean NDVI anomalies over the third and the fourth lagged months, that is,

$$N_{1,2} = \sum_{l=1}^2 \text{NDVI}_{m-l}/2,$$

$$N_{3,4} = \sum_{l=3}^4 \text{NDVI}_{m-l}/2, \tag{B1}$$

then Equation (3) can be rewritten as follows:

$$\bar{N} = (N_{1,2} + N_{3,4})/2,$$

$$N' = N_{1,2} - N_{3,4}. \tag{B2}$$

Equation (B2) suggests that $N_{1,2}$ and $N_{3,4}$ are equivalent to \bar{N} and N' . In fact, any linear combination of \bar{N} and N' can always be represented in terms of $N_{1,2}$ and $N_{3,4}$. To see this, suppose a_1 and a_2 are two constant coefficients (e.g., regression

Table B1. A recalculation of Table 2. OLS regression coefficients associated with $N_{1,2}$ and $N_{3,4}$ (Equation (B1)). Values in boldface or italics indicate that the results are significant at the 95% or 90% level, respectively.

	Jul	Aug	Sep	Oct
(a) NDVI Granger causes precipitation				
$N_{1,2}$	5.16	-1.02	0.53	-5.54
$N_{3,4}$	-3.72	-5.96	-4.06	3.35
(b) NDVI Granger causes temperature				
	Jul	Aug	Sep	Oct
$N_{1,2}$	-1.16	1.91	-1.85	-2.68
$N_{3,4}$	7.98	6.13	10.41	-3.28

coefficients) associated with \bar{N} and N' , respectively. From Equation (B2), the following relationships can be derived:

$$\begin{aligned}
 a_1\bar{N} + a_2N' &= a_1(N_{1,2} + N_{3,4})/2 + a_2(N_{1,2} - N_{3,4}) \\
 &= (a_1/2 + a_2)N_{1,2} + (a_1/2 - a_2)N_{3,4}.
 \end{aligned}
 \tag{B3}$$

Equation (B3) indicates that the regression coefficients of $N_{1,2}$ and $N_{3,4}$ can be directly calculated from those of \bar{N} and N' . In particular, when a_1 and a_2 have opposite signs (as in Table 2), they will reinforce each other to make the regression coefficient associated with $N_{3,4}$ larger (in absolute values). To some extent, this implies that more importance is put on $N_{3,4}$ as compared to $N_{1,2}$.

To verify the above relation, we test Granger causal relationships from $N_{1,2}$ and $N_{3,4}$ (instead of \bar{N} and N') upon both precipitation and temperature variability (Table B1). By comparing the results of Table B1 with Table 2, it is easy to verify that the regression coefficients in Table B1 and Table 2 satisfy the relationships described by Equation (B3). Also, Table B1 indicates that the causal influences of $N_{3,4}$ on climate variability are statistically more significant than those of $N_{1,2}$, and the signs associated with these coefficients suggest that higher vegetation anomalies earlier in the growing season (at lags of 3 or 4 months) may induce lower rainfall and higher temperature anomalies in late summer (July–September). As such, these results provide a complementary explanation for those of Table 2.

References

- Bonan, G. B., 2002: *Ecological Climatology, Concepts and Applications*. Cambridge University Press, 678 pp.
- , and L. M. Stillwell-Soller, 1998: Soil water and the persistence of floods and droughts in the Mississippi River Basin. *Water Resour. Res.*, **34**, 2693–2701.
- Bounoua, L., G. J. Collatz, S. O. Los, P. J. Sellers, D. A. Dazlich, C. J. Tucker, and D. A. Randall, 2000: Sensitivity of climate to changes in NDVI. *J. Climate*, **13**, 2277–2292.
- Bretherton, C. S., C. Smith, and J. M. Wallace, 1992: An intercomparison of methods for finding coupled patterns in climate data. *J. Climate*, **5**, 541–560.
- Churkina, G., and S. W. Running, 1998: Contrasting climatic controls on the estimated productivity of global terrestrial biomes. *Ecosystems*, **1**, 206–215.
- Czaja, A., and C. Frankignoul, 1999: Influence of the North Atlantic SST on the atmospheric circulation. *Geophys. Res. Lett.*, **26**, 2969–2972.

- , and —, 2002: Observed impact of Atlantic SST anomalies on the North Atlantic Oscillation. *J. Climate*, **15**, 606–623.
- Delire, C., J. A. Foley, and S. Thompson, 2004: Long-term variability in a coupled atmosphere–biosphere model. *J. Climate*, **17**, 3947–3959.
- Diebold, F. X., and R. S. Mariano, 1995: Comparing predictive accuracy. *J. Bus. Econ. Stat.*, **13**, 253–263.
- Enders, W., 1995: *Applied Econometric Time Series*. Wiley & Sons, 448 pp.
- Feteke, B. M., C. J. Vorosmarty, and W. Grabs, 2000: Global composite runoff fields based on observed river discharge and simulated water balances. UNH-GRDC Composite Runoff Fields v1.0, Complex Systems Research Center, University of New Hampshire, 120 pp.
- Fraedrich, K., A. Kleidon, and F. Lunkeit, 1999: A green planet versus a desert world: Estimating the effect of vegetation extremes on the atmosphere. *J. Climate*, **12**, 3156–3163.
- Friedl, M. A., and Coauthors, 2002: Global land cover mapping from MODIS: Algorithms and early results. *Remote Sens. Environ.*, **83**, 287–302.
- Gerten, D., S. Schaphoff, U. Haberlandt, W. Lucht, and S. Sitch, 2004: Terrestrial vegetation and water balance: Hydrological evaluation of a dynamic global vegetation model. *J. Hydrol.*, **286**, 249–270.
- Glendinning, P., 1994: *Stability, Instability, and Chaos: An Introduction to the Theory of Nonlinear Differential Equations*. Cambridge University Press, 388 pp.
- Granger, C. W. J., 1969: Investigating causal relations by econometric models and cross-spectral methods. *Econometrica*, **37**, 424–438.
- , 1980: Testing for causality: A personal viewpoint. *J. Econ. Dyn. Control*, **2**, 329–352.
- , and L. Huang, 1997: Evaluation of Panel Data Models: Some suggestions from time series. Department of Economics, University of California, San Diego, 29 pp.
- Hansen, J., R. Ruedy, J. Glascoe, and M. Sato, 1999: GISS analysis of surface temperature change. *J. Geophys. Res.*, **104**, 30 997–31 022.
- Heck, P., D. Luthi, and C. Schar, 1999: The influence of vegetation on the summertime evolution of European soil moisture. *Phys. Chem. Earth*, **24**, 609–614.
- , —, H. Wernli, and C. Schar, 2001: Climate impacts of European-scale anthropogenic vegetation changes: A sensitivity study using a regional climate model. *J. Geophys. Res.*, **106**, 7817–7835.
- Jenkins, G. M., and D. G. Watts, 1968: *Spectral Analysis and Its Applications*. Holden-Day, 525 pp.
- Kaufmann, R. K., and D. I. Stern, 1997: Evidence for human influence on climate from hemispheric temperature relations. *Nature*, **388**, 39–44.
- , L. Zhou, Y. Knyazikhin, N. V. Shabanov, R. B. Myneni, and C. J. Tucker, 2000: Effect of orbital drift and sensor changes on the time series of AVHRR vegetation index data. *IEEE Trans. Geosci. Remote Sens.*, **38**, 2584–2597.
- , —, R. B. Myneni, C. J. Tucker, D. Slayback, N. B. Shabanov, and J. Pinzon, 2003: The effect of vegetation on surface temperature: A statistical analysis of NDVI and climate data. *Geophys. Res. Lett.*, **30**, 2147, doi:10.1029/2003GL018251.
- , R. D. d’Arrigo, C. Laskowski, R. B. Myneni, L. Zhou, and N. J. Devi, 2004: The effect of growing season and summer greenness on northern forests. *Geophys. Res. Lett.*, **31**, L09205, doi:10.1029/2004GL019608.
- Kleidon, A., K. Fraedrich, and M. Heimann, 2000: A green planet versus a desert world: Estimating the maximum effect of vegetation on the land surface climate. *Climate Change*, **44**, 471–493.
- Koster, R. D., and Coauthors, 2004: Regions of strong coupling between soil moisture and precipitation. *Science*, **305**, 1138–1140.
- Kutzbach, J. E., 1967: Empirical eigenvectors of sea-level pressure, surface temperature and precipitation complexes over North America. *J. Appl. Meteor.*, **6**, 791–802.
- Los, S. O., 1998: Estimation of the ratio of sensor degradation between NOAA AVHRR channels 1 and 2 from monthly NDVI composites. *IEEE Trans. Geosci. Remote Sens.*, **36**, 206–213.

- Lotsch, A., M. A. Friedl, B. T. Anderson, and C. J. Tucker, 2003: Coupled vegetation-precipitation variability observed from satellite and climate records. *Geophys. Res. Lett.*, **30**, 1774, doi:10.1029/2003GL017506.
- Montaldo, N., R. Rondena, J. D. Albertson, and M. Mancini, 2005: Parsimonious modeling of vegetation dynamics for ecohydrologic studies of water-limited ecosystems. *Water Resour. Res.*, **41**, W10416, doi:10.1029/2005WR004094.
- Myneni, R. B., C. J. Tucker, G. Asrar, and C. D. Keeling, 1998: Interannual variations in satellite-sensed vegetation index data from 1981 to 1991. *J. Geophys. Res.*, **103** (D6), 6145–6160.
- Pal, J. S., and E. A. B. Eltahir, 2001: Pathways relating soil moisture conditions to future summer rainfall within a model of the land-atmosphere system. *J. Climate*, **14**, 1227–1242.
- Pielke, R. A., R. Avissar, M. Raupach, A. J. Dolman, X. Zeng, and A. S. Denning, 1998: Interactions between the atmosphere and terrestrial ecosystems: Influence on weather and climate. *Global Change Biol.*, **4**, 461–475.
- Pinzon, J. E., J. F. Pierce, and C. J. Tucker, 2001: Analysis of remote sensing data using Hilbert-Huang transform. *Proc. SCI 2001*, Orlando, FL, International Institute of Informatics and Systematics, 78–83.
- Richman, M. B., 1986: Rotation of principal components. *J. Climatol.*, **6**, 293–335.
- Salvucci, G. D., J. A. Saleem, and R. K. Kaufmann, 2002: Investigating soil moisture feedbacks on precipitation with tests of Granger causality. *Adv. Water Resour.*, **25**, 1305–1312.
- Sellers, P. J., and Coauthors, 1997: Modeling the exchanges of energy, water, and carbon between continents and the atmosphere. *Science*, **275**, 502–509.
- Shukla, J., and Y. Mintz, 1982: Influence of land-surface evapotranspiration on the Earth's climate. *Science*, **215**, 1498–1501.
- Trenberth, K. E., and D. J. Shea, 2005: Relationships between precipitation and surface temperature. *Geophys. Res. Lett.*, **32**, L14703, doi:10.1029/2005GL022760.
- Tucker, C. J., J. E. Pinzon, M. E. Brown, D. Slayback, E. W. Pak, R. Mahoney, E. Vermote, and N. El Saleous, 2005: An extended AVHRR 8-km NDVI data set compatible with MODIS and SPOT vegetation NDVI data. *Int. J. Remote Sens.*, **26**, 4485–4498.
- Vermote, E., and Y. J. Kaufman, 1995: Absolute calibration of AVHRR visible and near-infrared channels using ocean and cloud views. *Int. J. Remote Sens.*, **16**, 2317–2340.
- Wang, W., B. T. Anderson, R. K. Kaufmann, and R. B. Myneni, 2004: The relation between the North Atlantic Oscillation and SSTs in the North Atlantic basin. *J. Climate*, **17**, 4752–4759.
- , —, D. Entekhabi, D. Huang, R. K. Kaufmann, C. Potter, and R. B. Myneni, 2006: Feedbacks of vegetation on summertime climate variability over the North America Grasslands. Part II: A coupled stochastic model. *Earth Interactions*, in press.
- Weaver, J. E., 1954: *North American Prairie*. Johnsen Publishing Company, 348 pp.
- Wever, L. A., L. B. Flanagan, and P. J. Carlson, 2002: Seasonal and interannual variation in evapotranspiration, energy balance and surface conductance in a northern temperate grassland. *Agric. For. Meteorol.*, **112**, 31–49.
- Woodward, F. I., 1987: *Climate and Plant Distribution*. Cambridge University Press, 174 pp.
- Wu, W., M. A. Geller, and R. E. Dickinson, 2002: The response of soil moisture to long-term variability of precipitation. *J. Hydrometeorol.*, **3**, 604–613.
- Xie, P., and P. A. Arkin, 1997: Global precipitation: A 17-year monthly analysis based on gauge observations, satellite estimates, and numerical model outputs. *Bull. Amer. Meteor. Soc.*, **78**, 2539–2558.
- Zeng, N., H. Qian, C. Roedenbeck, and M. Heimann, 2005: Impact of 1998–2002 midlatitude drought and warming on terrestrial ecosystem and the global carbon cycle. *Geophys. Res. Lett.*, **32**, L22709, doi:10.1029/2005GL024607.

- Zhou, L., C. J. Tucker, R. K. Kaufmann, D. Slayback, N. V. Shabanov, and R. B. Myneni, 2001: Variations in northern vegetation activity inferred from satellite data of vegetation index during 1981 to 1999. *J. Geophys. Res.*, **106**, 20 069–20 083.
- , R. K. Kaufmann, Y. Tian, R. B. Myneni, and C. J. Tucker, 2003: Relation between interannual variations in satellite measures of northern forest greenness and climate between 1982 and 1999. *J. Geophys. Res.*, **108**, 4004, doi:10.1029/2002JD002510.

Earth Interactions is published jointly by the American Meteorological Society, the American Geophysical Union, and the Association of American Geographers. Permission to use figures, tables, and *brief* excerpts from this journal in scientific and educational works is hereby granted provided that the source is acknowledged. Any use of material in this journal that is determined to be “fair use” under Section 107 or that satisfies the conditions specified in Section 108 of the U.S. Copyright Law (17 USC, as revised by P.L. 94-553) does not require the publishers’ permission. For permission for any other form of copying, contact one of the copublishing societies.
